**NUCLEAR
INSTRUMENTS
& METHODS
IN PHYSICS
RESEARCH**
Section A

# Performance of a highly segmented scintillating fibres electromagnetic calorimeter

A. Asmone, M. Bertino, C. Bini, G. De Zorzi, G. Diambrini Palazzi, G. Di Cosimo, A. Di Domenico, F. Garufi, P. Gauzzi and D. Zanello

*Dipartimento di Fisica, Università "La Sapienza", Roma and INFN, Sezione di Roma, Roma, Italy*

A prototype of scintillating fibres electromagnetic calorimeter has been constructed and tested with 2, 4 and 8 GeV electron beams at the CERN PS. The calorimeter modules consist of a Bi–Pb–Sn alloy and scintillating fibres. The fibres are parallel to the modules longer axis, and nearly parallel to the incident electrons direction. The calorimeter has two different segmentation regions of $24 \times 24$ mm$^2$ and $8 \times 24$ mm$^2$ cross area respectively. Results on energy and impact point space resolution are obtained and compared for the two different granularities.

## 1. Introduction

Scintillating fibres calorimetry has developed into an extensive field [1].

The main purpose of the R&D program in e.m. calorimetry carried on by our group is to optimize a SCIFI calorimeter structure for what concerns the single-shower impact point precision and the multi-showers resolution [2]. These features are of great interest for e.m. calorimetry at future very high energy accelerators.

A modular calorimeter prototype has been constructed in Rome and tested at the electron beam T7 of the CERN PS at the end of 1991 [3]. This detector has been designed as an improved version of the calorimeter already used in the LEP-5 experiment in 1990/91 [4,5].

In this paper we are reporting on its performance concerning energy resolution and impact point precision.

## 2. The calorimeter

The calorimeter modules are made of a high density and low melting point alloy (52.5% Bi + 32.0% Pb + 15.5% Sn, in weight) and 1 mm diameter scintillating fibres parallel to the module longer axis, and at a small angle to the incident electrons. The filling factor (= fibres volume/total volume) is 19.5%, and the module length is 35 cm corresponding to 38 R.L.

In the central region, as can be seen in the sketch of fig. 1, each module ($24 \times 24$ mm$^2$) is divided in three

$8 \times 24$ mm$^2$ submodules. This structure is not mechanical but only optical and is obtained by sending three separate fibre bundles to three different PMTs. In this way an 8 mm granularity is achieved in the $x$ (horizontal) coordinate.

The calorimeter main features are summarized in table 1.

The alloy melting point is 96°C. This allows to employ a simple fusion technique. 144 stainless steel tubes (1.1 mm internal, 1.5 mm external diameter) are held in position by two steel plates at the extremities of an aluminium cast. The liquefied alloy is poured inside the cast. The low melting temperature of this alloy allowed us to achieve a more satisfactory mechanical precision for the modules with respect to the "pure lead" fusion technique previously employed [5].

Each fibre bundle (48 fibres in a central module, 144 fibres in a peripherical module) is glued to a light pipe. The pipe square cross area has been optimized in order to get a uniform light collection over the whole fibre bundle.

A yellow optical filter is interposed between the light pipe and the PMT in order to improve the attenuation length of the scintillating fibres with a tolerable loss in the total light collection.

The PMT outputs are sent to fast 11 bits 16 channels ADC's (LeCroy 4300B/610 FERA).

## 3. Test and results

A test has been performed in december 1991 at the CERN PS on the T7-South beam with electrons of 2,4
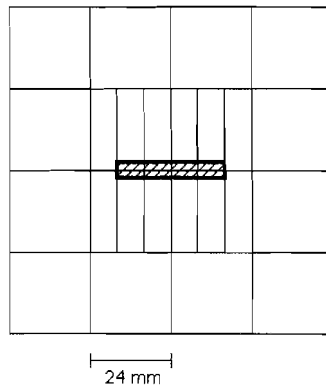
Fig. 1. Sketch of the calorimeter front view; the highly segmented central region 8 mm (horizontal)×24 mm (vertical) is shown. The hatched area corresponds to the region scanned by the e⁻ beam.

and 8 GeV energy. The detector was placed on a movable platform allowing the horizontal scan of the beam (see fig. 1), as well as a vertical tilt with respect to the beam.

The effective beam horizontal size was reduced to less than 1 mm by gating the calorimeter signals with the coincidence of two crossed scintillation counters; the horizontal one is 5 mm high and the vertical one is a single 1 mm diameter fibre. Furthermore a telescope of two beam chambers 2 m apart has been used to measure the direction of the incident electrons; their spatial accuracy is of the order of 0.2 mm. The calorimeter was mainly operated at a vertical tilt angle of 2.5° respect to the electron beam (this value is not optimized).
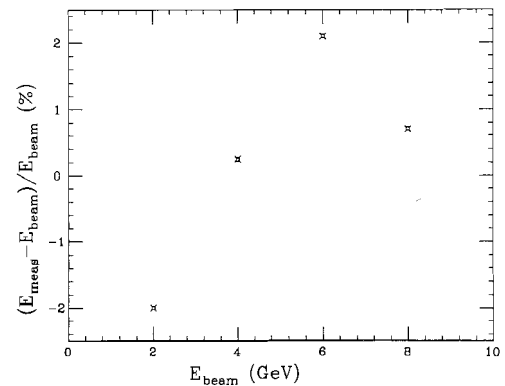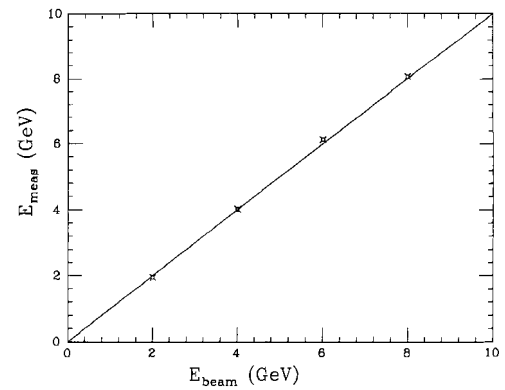


Fig. 2. Measured energy vs nominal beam energy (vertical tilt angle = 2.5°); the energy response is linear within ±2%.

### 3.1. Energy resolution

The calorimeter energy response turns out to be linear within 2% in the explored energy range, as shown in fig. 2.

Table 1
Calorimeter's main features

| Scintillating fibres | Kuraray SCSF-81 of 1 mm diameter |
|---|---|
| Absorber alloy (% in weight) | AF-17 (52.5% Bi + 32.0% Pb + 15.5%Sn) |
| Filling factor | 19.5% |
| Average density | 7.6 g/cm³ |
| Average radiation lenght | 0.91 cm |
| Read-out PMT | XP1911 |
| PMT photocathode diameter | 14 mm |
| Optical filter | Kodak Wratten No. 8 |
| Total number of read-out channels | 24 |
| Mechanical module cross area | 24×24 mm² |
| Central module cross area | 8 (horizontal)×24 (vertical) mm² |
| Number of fibres per central module | 48 ( = 4 (horizontal)×12 (vertical)) |
| Calorimeter total cross area | 96×96 mm² |
| Calorimeter total lenght | 350 mm |

The energy resolution $\sigma/E$ is a linear function of $1/\sqrt{(E(\text{GeV}))}$. In fig. 3 the results are presented at $0°$ and $2.5°$ vertical tilt angle. They are comparable, but resolutions at $0°$ are larger probably due to electron channeling. By fitting the data we get:

$0°$: $\sigma/E = 18.5\%/\sqrt{(E(\text{GeV}))} + 1.9\%$,

$2.5°$: $\sigma/E = 16.0\%/\sqrt{(E(\text{GeV}))} + 1.6\%$.

This resolution can be compared to similar results of other calorimeters having approximatively the same filling factor and tilt angle [1], and appears to be slightly worse.

However residual mechanical imperfections, non-uniform light collection from fibres bundles to PMTs, intercalibration of the many modules collecting the energy of a shower, and reduced photoelectron statistics due to the small number of fibres per module (and to the optical filter) can account for this worsening. This modest worsening may be the price we pay for our high segmentation.

In a special run at 4 GeV with $2.5°$ tilt the calorimeter signal was gated with a "short" pulse. Under these conditions the ADC integrates essentially the first 5 ns of the signal, corresponding to the pulse rise time (Notice that this rise-time is mainly determined by the PMT itself and would be shorter with a faster PMT). The energy resolution turns out to be worse by about 30% with respect to the full gate.

In fig. 4 the calorimeter response uniformity is shown at 8 GeV. A horizontal scanning through four adjacent modules was done as shown in fig. 1. A small disuniformity (7%) is visible between two modules which are "mechanically" separated, due to residual mechanical imperfections. No similar effect is seen between modules only "optically" separated.

### 3.2. Spatial resolution

The horizontal position $x$ of an electron showering in the calorimeter can be determined in a simple way by the centre of gravity $\langle x \rangle$ of the energy deposited in the various modules. The resulting precision of this quantity both for large and small modules is shown in figs. 5a and 6a respectively, where the "true" $x$-coordinate is measured with the beam chambers. The waving behaviour of these data distributions is typical of all calorimeters with finite size modules.

Better results are obtained using a special reconstruction algorithm as shown in figs. 5b and 6b. This correcting procedure is similar to many others used by different authors [6]. Whereas these authors use exponential functions to represent the transverse energy shower distribution, in this case a gaussian is employed [5].
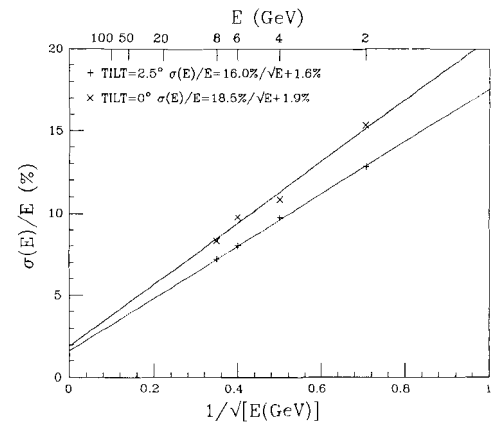


Fig. 3. Energy resolution $\sigma/E$ as a function of $1/\sqrt{(E(\text{GeV}))}$ for two different vertical tilt angles ($0°$ and $2.5°$).

The method was derived in the following way. Under the approximation that the transverse energy distribution of a shower can be represented by a two-dimensional gaussian function, the behaviour of $\langle x \rangle$ as a function of $x$ can be described by a function of $x$
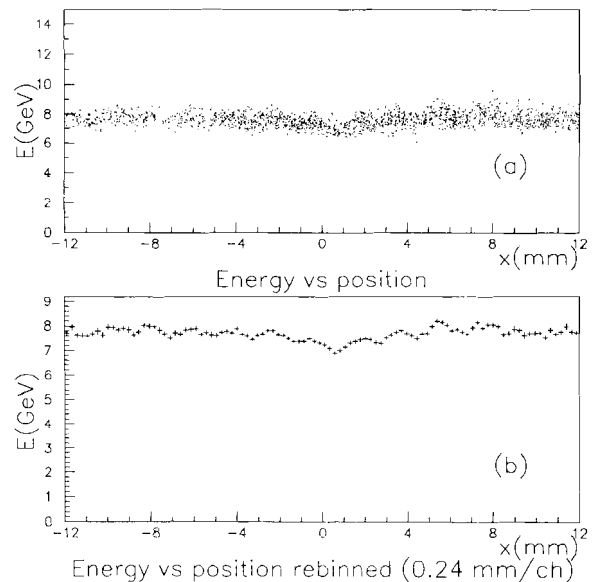


Fig. 4. (a) Calorimeter response uniformity shown at 8 GeV. A horizontal scanning was carried on through four adjacent small modules. At the axis origin a small disuniformity (7%) is visible between two modules which are "mechanically" separated. No similar effect is seen between modules only "optically" separated. (b) Same data rebinned in order to show the periodicity of the single fibre position. The peak to peak distance corresponds to the fibre periodicity.

which contains as a free parameter only the width $\rho$ of the gaussian itself:

$$\langle x \rangle = \ell + 4\ell \, \exp\left(-2\ell^2/\rho^2\right)$$

$$\times \frac{\sinh\left[2\ell(x-\ell)/\rho^2\right]}{1 + 2\exp\left(-2\ell^2/\rho^2\right)\cosh\left[2\ell(x-\ell)/\rho^2\right]}$$

where $2\ell$ is the module dimension and $\rho$ is the parameter to be determined. By fitting the data with this function this parameter is fixed. By inverting the function a better estimate $\langle x \rangle_{corr}$ for $x$ is obtained. The fitted gaussian width does not depend on energy in the explored range.

The precision in reconstructing the impact point of the electronic shower in the horizontal $x$-coordinate at 8 GeV is illustrated by figs. 7 and 8 for large and small modules respectively. Here the events distribution is plotted versus the difference between calorimeter-reconstructed and beam chambers measured $x$-coordinate.
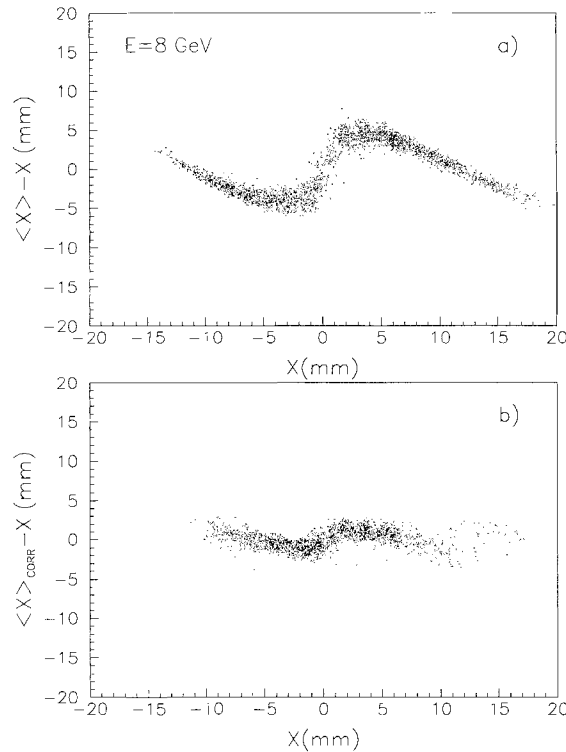


Fig. 5. (a) Comparison between reconstructed $\langle x \rangle$ and "true" $x$ at 8 GeV. $x$ is measured with the beam wire chambers. $\langle x \rangle$ is determined as the "centre of gravity" of the energy deposited in the various calorimeter 24×24 mm² modules. (b) Comparison between reconstructed $\langle x \rangle_{corr}$ and "true" $x$ at 8 GeV. $\langle x \rangle_{corr}$ is determined by the algorithm described in section 3.2. The waving behaviour shown in (a) is now greatly diminished.
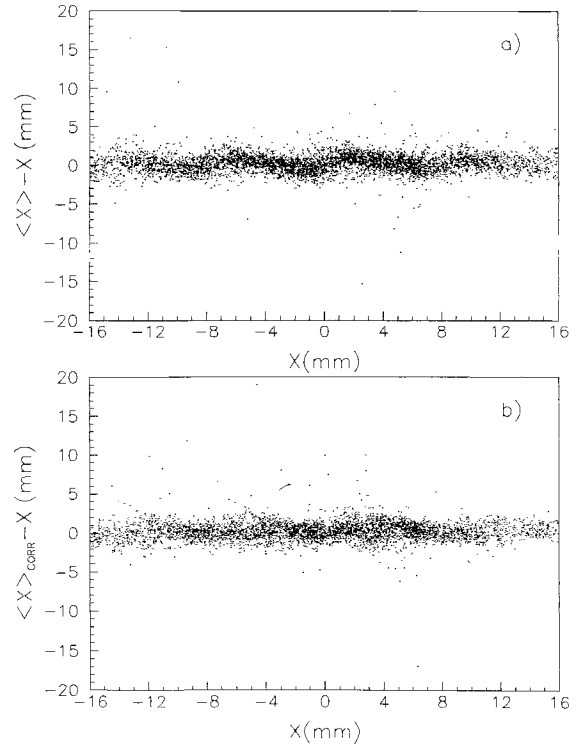


Fig. 6. (a) Same as in fig. 5a for the 8×24 mm² modules. (b) Same as in fig. 5b for the 8×24 mm² modules. For the smaller modules the waving behaviour is essentially suppressed.

By fitting the experimental data with a gaussian function, $\sigma_x$ is evaluated at various electron energies.

The effect of the algorithm is to render the spatial resolution quasi-independent on the impact $x$-coordinate.

The space resolution has been analysed both for small (8 × 24 mm²) and large (24 × 24 mm²) modules. The larger segmentation is obtained by adding the signals from three adjacent modules.

As shown in fig. 9, $\sigma_x$ turns out to be a linear function of $1/\sqrt{(E(\text{GeV}))}$. Experimental points are obtained analysing the data with the algorithm previously described. The beam chamber contribution to the error is not subtracted. We obtain:

$$\sigma_x = 2.8 \text{ mm}/\sqrt{(E(\text{GeV}))} + 0.07 \text{ mm},$$

for small modules,

$$\sigma_x = 2.7 \text{ mm}/\sqrt{(E(\text{GeV}))} + 0.6 \text{ mm},$$

for large modules.

For the small modules the energy independent term is compatible with the beam chambers resolution. For the large modules the constant term is due mainly to a
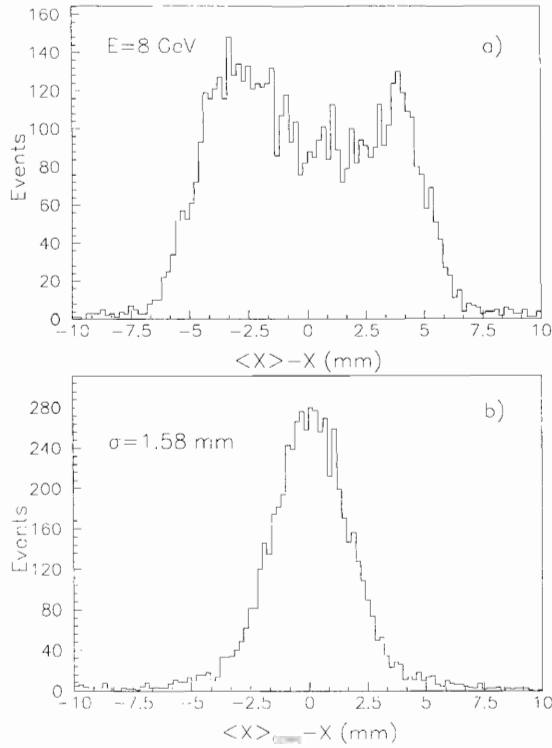
Fig. 7. Impact point distribution as a function of the difference between the calorimeter reconstructed abscissa and the "true" one at 8 GeV for the large modules. (a) By a simple "centre of gravity" reconstruction the distribution is nongaussian and a $\sigma_x$ cannot be given, as expected also from the distribution shown in fig. 5a. (b) Using the algorithm described in section 3.2. and by fitting a Gaussian function one finds $\sigma_x = 1.58$ mm.
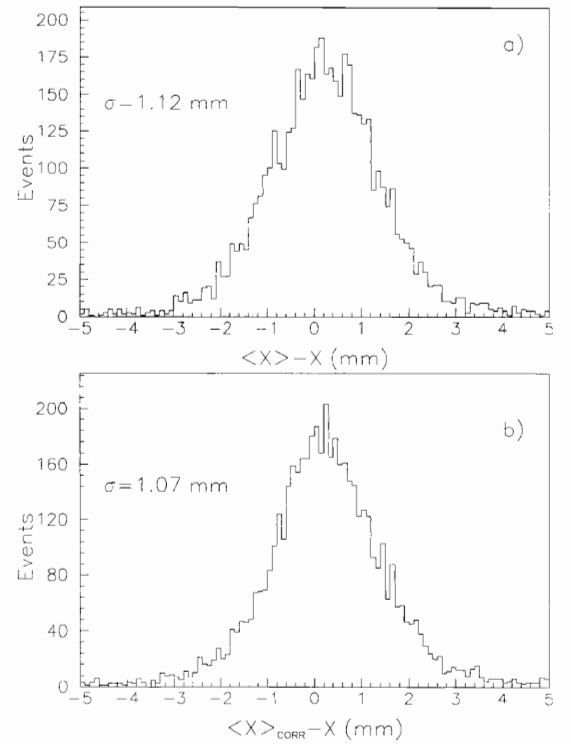
Fig. 8. Same as in fig. 7 for small modules. (a) impact point distribution at 8 GeV as a function of ($\langle x \rangle - x$). By fitting a gaussian function one finds $\sigma_x = 1.12$ mm. This result is obtained using the simple "centre of gravity" algorithm (see figs. 5a and 7a). (b) Impact point distribution at 8 GeV as a function of ($\langle x \rangle_{corr} - x$). By fitting a gaussian function $\sigma_x = 1.07$ mm is obtained.

residual waving behaviour of the reconstructed $\langle x \rangle_{corr}$ coordinate (see fig. 5b).

The special "short gate" run at 4 GeV (see section 3.1) shows that the spatial resolution is not worsened by gating the 5 ns rise-time of the calorimeter signal.

## 4. Conclusions

We have constructed a modular e.m. calorimeter and performed a test with electrons from 2 to 8 GeV energy. The main purpose was to study and improve the spatial resolution i.e. the impact point recontruction of a single e.m. shower. A module cross area is $24 \times 24$ mm$^2$, and $8 \times 24$ mm$^2$ in the calorimeter central region. The calorimeter was operated at a vertical tilt angle of 2.5° with respect to the electron beam. The energy resolution turns out to be: $\sigma/E = 16.0\%/\sqrt{(E(\text{GeV}))} + 1.6\%$. The impact point horizontal res-
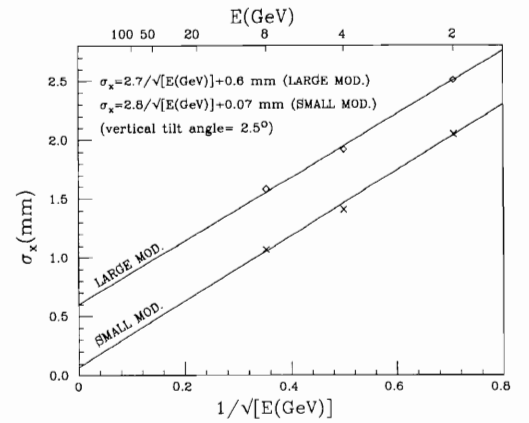


Fig. 9. Impact point resolution of the electron shower $\sigma_x$ as a function of the electron energy. Experimental points are obtained analysing the data with the algorithm described in section 3.2. both for small and large modules. A contribution to the energy-independent term of the order of 0.1 mm is compatible with the beam chambers resolution. Notice that the vertical tilt angle is 2.5°.

olution is: $\sigma_x = 2.8$ mm $/\sqrt{V(E(\text{GeV}))} + 0.07$ mm and $\sigma_x = 2.7$ mm $/\sqrt{(E(\text{GeV}))} + 0.6$ mm for a module horizontal size of 8 mm and 24 mm respectively. The spatial resolution does not depend on the impact point of the shower, when an appropriate algorithm is employed in reconstructing the impact position of the electron. Furthermore it is interesting that gating the calorimeter signal only during the pulse rise-time, the energy resolution $\sigma/E$ is worsened (about 30%), while the spatial resolution $\sigma_x$ is unaffected.

## Acknowledgements

## References

[1] The most significant results come from the SPACAL collaboration at CERN and have been reviewed by R. Wigmans, talk given at 5th Pisa Meeting on Advanced Detectors, La Biodola, Isola d'Elba, Italy, eds. A. Baldini, A. Scribano and G. Tonelli, Nucl. Instr. and Meth. A 315 (1992) 299.
[2] R&D experiment FIB has been supported by INFN (Italy) in 1991/92.
[3] A preliminary version of this paper has appeared as a preprint: A. Asmone et at., CERN-PPE/92-67, 4 March 1992.
[4] C. Bini et al., Nucl. Instr. and Meth. A 306 (1991) 467.
[5] M. Bertino et al., Proc. 5th Pisa Meeting on Advanced Detectors, La Biodola, Isola d'Elba, Italy, May 1991, eds. A. Baldini, A. Scribano and G. Tonelli, Nucl. Instr. and Meth. A 315 (1992) 327.
[6] G.A. Akopdjanov et al., Nucl. Instr. and Meth. 140 (1977) 441;
D. Acosta et al., Nucl. Instr. and Meth. A 305 (1991) 55.